ELSEVIER

Journal of Magnetism and Magnetic Materials 246 (2002) 366–374

Journal of magnetism and magnetic materials

www.elsevier.com/locate/jmmm

Magnetic ordering in the ternary germanide $Ce_2Ni_3Ge_5$ as studied by neutron powder diffraction

L. Durivault[a,b], F. Bourée[a], B. Chevalier[b,*], G. André[a], J. Etourneau[b]

[a] *Laboratoire Léon Brillouin (CEA-CNRS), CEA/Saclay, 91191 Gif-sur-Yvette, France*

[b] *Institut de Chimie de la Matière Condensée de Bordeaux (ICMCB), CNRS [UPR 9048], Université de Bordeaux I, 87 Avenue du Dr. A. Schweitzer, 33608 Pessac, France*

Received 6 September 2001; received in revised form 20 November 2001

Abstract

Neutron powder diffraction investigations on $Ce_2Ni_3Ge_5$ have been carried out. This compound adopts the $U_2Co_3Si_5$-type structure (Ibam space group) with only one crystallographic site available for Ce atoms. Magnetisation measurements indicate that $Ce_2Ni_3Ge_5$ undergoes two antiferromagnetic transitions at low temperature, at $T_{N1} = 4.8(2)$ K and $T_{N2} = 4.2(2)$ K, respectively. From our neutron diffraction experiments, only one transition is evidenced, below T_{N1}, $Ce_2Ni_3Ge_5$ is a collinear antiferromagnet with magnetic moments parallel to the **a**-axis and equal to $0.4(1)\,\mu_B$/Ce at $T = 1.4$ K.

PACS: 61.12; 75.50.E

Keywords: Ternary germanide; Antiferromagnet; Magnetic structure; Kondo effect

1. Introduction

During the last decade, the existence of many ternary silicides $Ce_2M_3Si_5$ and germanides $Ce_2M_3Ge_5$ based on M = 3d, 4d or 5d transition elements and crystallising in the orthorhombic $U_2Co_3Si_5$-type structure, for instance $Ce_2Ni_3Si_5$ [1], $Ce_2Ni_3Ge_5$ [2], $Ce_2Rh_3Si_5$ (or Ge_5) [3], $Ce_2Ir_3Si_5$ (or Ge_5) [3] and $Ce_2Pd_3Ge_5$ [4] was reported. It should be noted that the $U_2Co_3Si_5$-type presents structural similarities with the tetragonal $ThCr_2Si_2$-type found for the ternary compounds CeM_2Si_2 and CeM_2Ge_2. Both $Ce_2M_3Si_5$ and $Ce_2M_3Ge_5$ intermetallics were intensively investigated due to interesting physical properties; $Ce_2Ni_3Si_5$, $Ce_2Rh_3Si_5$ and $Ce_2Ir_3Si_5$ are intermediate valence materials [3,5] whereas $Ce_2Rh_3Ge_5$ and $Ce_2Ir_3Ge_5$ are antiferromagnetically ordered Kondo systems showing a moderate heavy-fermion behaviour [6].

Recently, the magnetisation measurements on $Ce_2Ni_3Ge_5$ revealed antiferromagnetic ordering below $T_N = 4.2$ K [7]. Later, specific heat measurements performed on this ternary germanide have shown two successive peaks at $T_{N1} = 5.1$ K and $T_{N2} = 4.5$ K attributed to the existence of two antiferromagnetic transitions [8]. Moreover, this

*Corresponding author. Tel.: +33-5-56-84-63-36; fax: +33-5-56-84-27-61.

E-mail address: chevalie@icmcb.u-bordeaux.fr (B. Chevalier).

0304-8853/02/$ - see front matter
PII: S0304-8853(02)00107-5

last study indicates a considerable reduction of the magnetic entropy at T_{N1} suggesting a small value for the ordered magnetic moment (Kondo effect). In this view, it seemed necessary to determine the magnetic structure of $Ce_2Ni_3Ge_5$. We can recall also that in the Ce–Ni–Ge system, the ternary germanide $Ce_2Ni_3Ge_5$ is close to $CeNi_2Ge_2$ exhibiting the signature of superconductivity at ambient pressure or under pressure [9,10].

In this paper, we report on $Ce_2Ni_3Ge_5$ crystal and magnetic structures as determined by neutron powder diffraction.

2. Experimental procedures

A polycrystalline sample of $Ce_2Ni_3Ge_5$ was prepared by melting stoichiometric amounts of the constituents (purity, 99.9%) in an induction levitation furnace under a purified argon atmosphere. Ingot was sealed under vacuum in quartz tube and was annealed at 1073 K for 34 days.

The homogeneity and chemical composition were checked before and after annealing by microprobe analysis as previously described [11]. The "as-cast" sample is a mixture containing three phases: $Ce_2Ni_3Ge_5$, $CeNiGe_2$ and NiGe. This result indicates clearly that the ternary germanide $Ce_2Ni_3Ge_5$ does not melt congruently. On the contrary, the annealed sample exhibits a good chemical homogeneity and is single phase.

Magnetisation measurements were carried out using a superconducting quantum interference device (SQUID) magnetometer.

Neutron powder diffraction experiments were performed at the Orphée reactor (CEA/Saclay, France), on the two-axis diffractometers 3T2 (high-resolution powder diffraction; $\lambda = 0.1225$ nm) and G4-1 (800 cell-Position-Sensitive Detector; $\lambda = 0.2426$ nm). The data were analysed with the Rietveld profile method [12] using the Fullprof program [13], with neutron scattering lengths and Ce^{3+} form factor, respectively, from Refs. [14,15].

3. Results and discussion

3.1. Magnetisation measurement

Fig. 1 presents the thermal dependence of the magnetisation M of $Ce_2Ni_3Ge_5$ measured in an

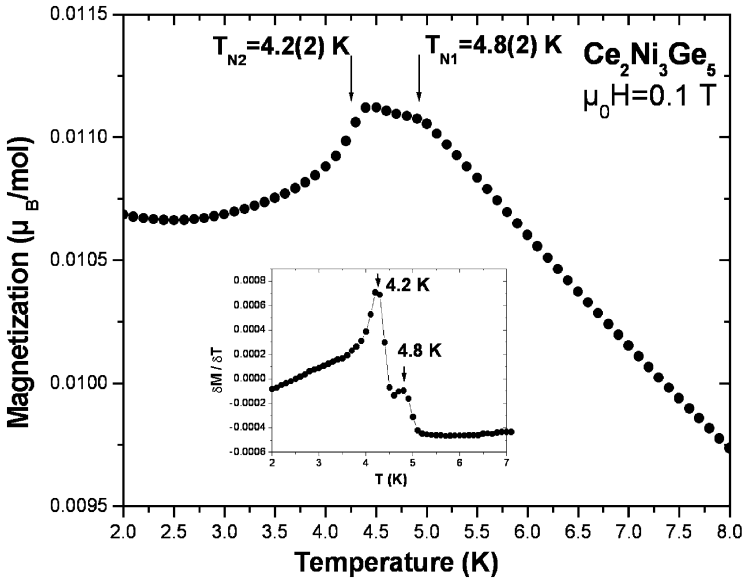

Fig. 1. Thermal dependence of the magnetisation of $Ce_2Ni_3Ge_5$ at low temperatures measured in an applied field of $\mu_0 H = 0.1$ T. The inset shows the corresponding derivative curve.

applied field of 0.1 T. Two maxima are clearly visible on the derivative curve $dM/dT = f(T)$ (inset of Fig. 1): a smaller one occurring at $T_{N1} = 4.8(2)$ K and a larger one at $T_{N2} = 4.2(2)$ K. These two temperatures are correlated to a change of slope and a decrease in the curve $M = f(T)$. This behaviour is similar to that observed by Hossain et al. [8] but with systematically smaller values for T_{N1} and T_{N2}.

3.2. Neutron powder diffraction

Neutron diffraction peaks observed at 300 K confirm that $Ce_2Ni_3Ge_5$ crystallises in the orthorhombic $U_2Co_3Si_5$-type structure (space group Ibam). No trace of any impurity phase was observed in the diagram. The Rietveld profile refinement of the diffraction data is represented in Fig. 2. The lattice parameters $a = 0.98085(2)$ nm, $b = 1.18378(3)$ nm and $c = 0.59602(1)$ nm are in good agreement with those reported earlier [2,8]. The results of the refinement (positional and isotropic thermal parameters) are collected in Table 1.

A partial representation of the crystal structures of $Ce_2Ni_3Ge_5$ and $CeNi_2Ge_2$ is shown in Fig. 3. It is worthwhile noting that the $Ce_2Ni_3Ge_5$ orthorhombic structure derives from the $CeNi_2Ge_2$ tetragonal structure ($ThCr_2Si_2$-type) [16]. This last structure is a stacking of layers consisting of $[Ce_4Ni_4]$ antiprisms containing Ge atoms; the $Ce_2Ni_3Ge_5$ orthorhombic structure results from a stacking of two distorted $[Ce_4Ge(1)_2Ge(2)_2]$ and

Table 1
Positional and isotropic thermal parameters for $Ce_2Ni_3Ge_5$ (Ibam space group) at 300 K

Atom	Site	Positional parameters			Biso (Å^2)
		x	y	z	
Ce	8j	0.2627(3)	0.1320(3)	0	0.56(4)
Ni(1)	4a	0	0	$\frac{1}{4}$	0.89(4)
Ni(2)	8j	0.1093(1)	0.3661(2)	0	0.80(3)
Ge(1)	4b	$\frac{1}{2}$	0	$\frac{1}{4}$	0.45(4)
Ge(2)	8g	0	0.2346(1)	$\frac{1}{4}$	0.74(3)
Ge(3)	8j	0.3480(2)	0.3968(1)	0	0.77(3)

The reliability factors are $R_{wp} = 9.4\%$ and $R_B = 4.9\%$, respectively.

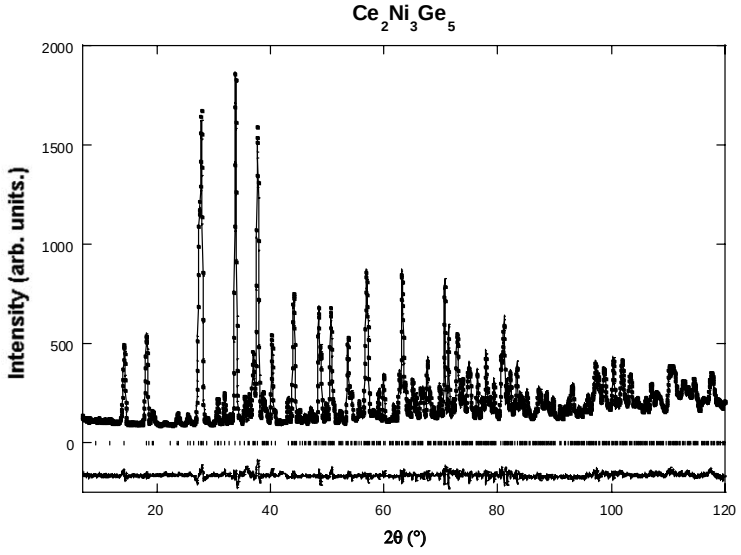

Fig. 2. Rietveld refinement diagram of $Ce_2Ni_3Ge_5$ germanide at 300 K ($\lambda = 0.1225$ nm). The dots represent the observed data points, the solid lines reveal the calculated profile and the difference (bottom) between observed and calculated profiles. The ticks correspond to 2θ Bragg positions.

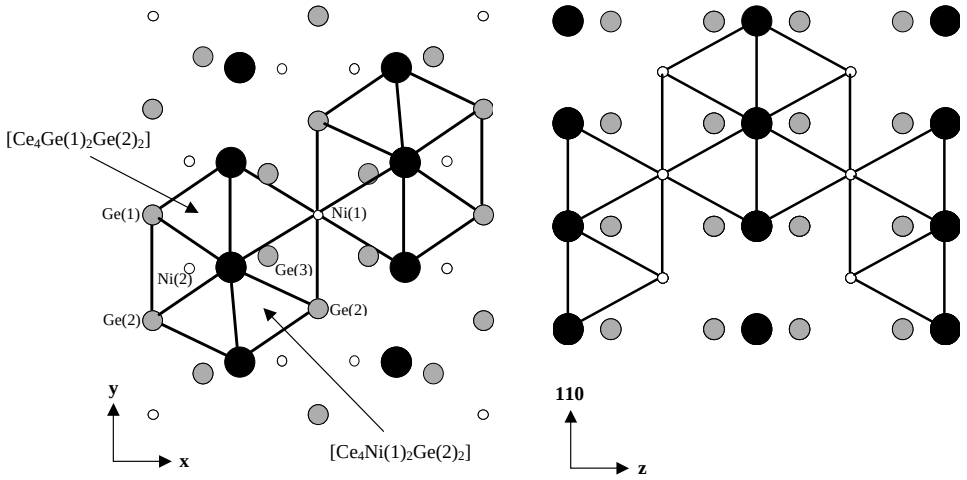

Fig. 3. (left) Crystal structure of $Ce_2Ni_3Ge_5$ projected onto the (0 0 1) plane (with crystallographic axis: $\mathbf{a_O}$, $\mathbf{b_O}$ and $\mathbf{c_O}$ in the orthorhombic space group Ibam). (right) Crystal structure of $CeNi_2Ge_2$ projected onto the (1 1 0) plane (with crystallographic axis: $\mathbf{a_T}$, $\mathbf{b_T}$ and $\mathbf{c_T}$ in the tetragonal space group I4/mmm). Ce, Ge and Ni are, respectively, represented by large black, medium grey and small white circles.

Table 2
Selected interatomic distances existing at $T = 300\,K$ in $CeNi_2Ge_2$ and $Ce_2Ni_3Ge_5$ (data relative to $CeNi_2Ge_2$ are taken from Ref. [17])

Germanide	d_{Ce-Ce} (nm)	d_{Ce-Ni} (nm)	d_{Ce-Ge} (nm)
$CeNi_2Ge_2$	Ce–4Ce 0.4150	Ce–8Ni 0.3221	Ce–8Ge 0.3183
$Ce_2Ni_3Ge_5$	Ce–2Ce 0.40925(5)	Ce–2Ni(1) 0.33618(5)	Ce–2Ge(1) 0.31749(5)
	Ce–2Ce 0.43184(5)	Ce–1Ni(2) 0.31534(5)	Ce–2Ge(2) 0.31831(5)
		Ce–2Ni(2) 0.32339(5)	Ce–2Ge(2) 0.32148(5)
		Ce–1Ni(2) 0.33889(5)	Ce–1Ge(3) 0.29885(5)
		Ce–1Ni(2) 0.33998(5)	Ce–2Ge(3) 0.31901(5)
			Ce–2Ge(3) 0.32444(5)

$[Ce_4Ni(1)_2Ge(2)_2]$ antiprisms surrounding Ni(2) and Ge(3) atoms, respectively. Considering the sequence $CeNi_2Ge_2 \rightarrow Ce_2Ni_3Ge_5$, the substitution of Ge(1) and Ge(2) atoms for Ni induces a deformation of the antiprisms. Another structural particularity is that the Ce atoms, which are located in planes perpendicular to the **c**-axis in $CeNi_2Ge_2$, form "wavy planes" perpendicular to **a**-axis in $Ce_2Ni_3Ge_5$.

It is worthwhile comparing the interatomic distances existing between Ce atom with Ni and Ge ligands in the two ternary germanides $CeNi_2Ge_2$ and $Ce_2Ni_3Ge_5$ (Table 2). Ce atoms in $CeNi_2Ge_2$ have 8 nickel and 8 germanium as first neighbours whereas in $Ce_2Ni_3Ge_5$ these two numbers are, respectively, equal to 7 and 10. The average interatomic distances $d_{Ce-Ni} = 0.3305\,nm$ and $d_{Ce-Ge} = 0.3176\,nm$ existing in $Ce_2Ni_3Ge_5$ are, respectively, greater and comparable to that observed in heavy-fermion compound $CeNi_2Ge_2$ (Table 2) [10]. This result indicates that the 4f(Ce)–4p(Ge) hybridisation may be considered in order to explain the physical properties of $Ce_2Ni_3Ge_5$.

Neutron powder diffraction patterns ($\lambda = 0.2426\,nm$) have been recorded in the 1.4–6 K low-temperature range (Fig. 4). At 6 K, the pattern reveals only nuclear reflections which are indexed in the orthorhombic unit cell having

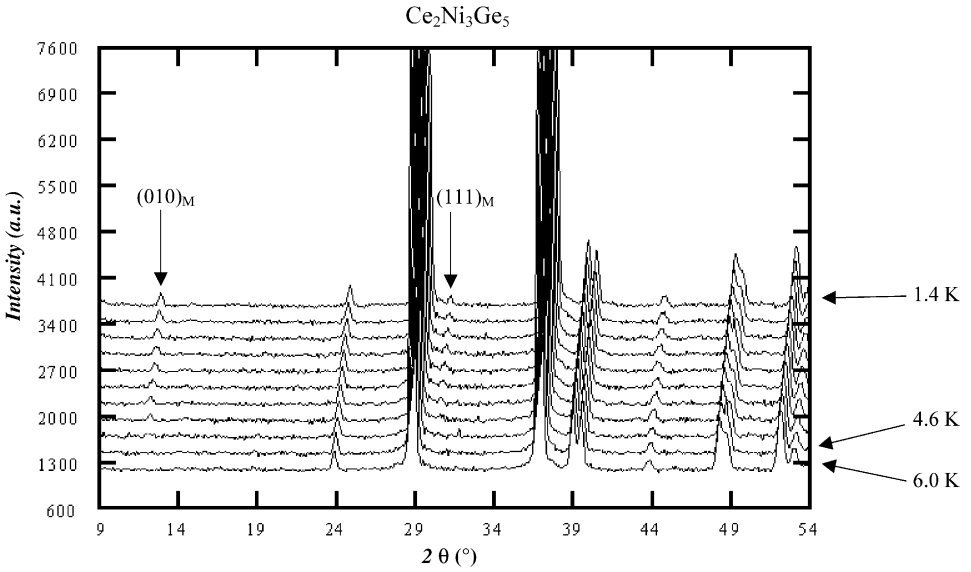

Fig. 4. $Ce_2Ni_3Ge_5$ neutron powder diffraction patterns ($\lambda = 0.2426$ nm) from 6 K (front of the figure) to 1.4 K (bottom of the figure). The magnetic peaks are labelled $(h\,k\,l)_M$.

Table 3
Bertaut's representation analysis of magnetic structures (Ibam space group, $\mathbf{k} = (0\,1\,0)$ propagation vector)

Representation	Ce(1) $[x\,y\,0]$			Ce(2) $[x\,-y\,]$			Ce(3) $[-x\,y\,\frac{1}{2}]$			Ce(4) $[-x\,-y\,0]$		
Γ_1			$+M_{z1}$			$-M_{z2}$			$-M_{z3}$			$+M_{z4}$
Γ_2	$+M_{x1}$	$+M_{y1}$		$+M_{x2}$	$-M_{y2}$		$-M_{x3}$	$+M_{y3}$		$-M_{x4}$	$-M_{y4}$	
Γ_3	$+M_{x1}$	$+M_{y1}$		$+M_{x2}$	$-M_{y2}$		$+M_{x3}$	$-M_{y3}$		$+M_{x4}$	$+M_{y4}$	
Γ_4			$+M_{z1}$			$-M_{z2}$			$+M_{z3}$			$-M_{z4}$
Γ_5	$+M_{x1}$	$+M_{y1}$		$-M_{x2}$	$+M_{y2}$		$-M_{x3}$	$+M_{y3}$		$+M_{x4}$	$+M_{y4}$	
Γ_6			$+M_{z1}$			$+M_{z2}$			$-M_{z3}$			$-M_{z4}$
Γ_7			$+M_{z1}$			$+M_{z2}$			$+M_{z3}$			$+M_{z4}$
Γ_8	$+M_{x1}$	$+M_{y1}$		$-M_{x2}$	$+M_{y2}$		$+M_{x3}$	$-M_{y3}$		$-M_{x4}$	$-M_{y4}$	

$a = 0.98148(8)$ nm, $b = 1.18080(9)$ nm and $c = 0.59560(4)$ nm as parameters . Below 4.6 K the patterns reveal two small additional reflections, $(0\,1\,0)_M$ and $(1\,1\,1)_M$, characteristic of antiferromagnetic order in a magnetic unit cell identical to the chemical unit cell. These peaks obey the selection rule $h + k + l = 2n + 1$ implying that two magnetic moments separated by $[\frac{1}{2}\frac{1}{2}\frac{1}{2}]$ are opposite. The propagation vector associated with $Ce_2Ni_3Ge_5$ antiferromagnetic order is $\mathbf{k} = (0\,1\,0)$.

The cerium atoms in $Ce_2Ni_3Ge_5$ unit cell (Ibam space group, (8j) Wyckoff site) are: Ce(1) with $[x\,y\,0]$; Ce(2) $[x\,-y\,\frac{1}{2}]$; Ce(3) $[-x\,y\,\frac{1}{2}]$; Ce(4) $[-x\,-y\,0]$; $x = 0.2627(3)$ and $y = 0.1320(3)$ (Table 1). Ce(5)–Ce(8) atoms are obtained from Ce(1)–Ce(4) atoms via $[\frac{1}{2}\frac{1}{2}\frac{1}{2}]$ translation. For Ibam space group, $\mathbf{k} = (0\,1\,0)$ propagation vector and (8j) Wyckoff position, as many as eight magnetic structures are obtained via Bertaut's representation analysis [18]. These magnetic structures are listed in Table 3: Ce(1)–Ce(4) magnetic moments only are indicated, the Ce($i+4$), $i = 1-4$, and Ce(i) magnetic moments being opposite.

In order to compare $Ce_2Ni_3Ge_5$ neutron powder diffraction experimental data [$(0\,1\,0)_M$ exists, no $(1\,0\,0)_M$ and $(0\,0\,1)_M$ magnetic Bragg peaks are

Table 4
Magnetic structure factor $\langle \mathbf{F}_M(\mathbf{K}) \cdot \mathbf{F}_M^*(\mathbf{K}) \rangle$ as calculated for Γ_1–Γ_8 magnetic structures (Table 3) for $(0\,1\,0)_M$, $(1\,0\,0)_M$ and $(0\,0\,1)_M$ Magnetic Bragg reflections

	$(0\,1\,0)_M$	$(1\,0\,0)_M$	$(0\,0\,1)_M$
Γ_1	0	0	0
Γ_2	0	0	0
Γ_3	$\cos^2(2\pi y_{Ce})M_x^2$	0	M_y^2
Γ_4	$\sin^2(2\pi y_{Ce})M_z^2$	0	0
Γ_5	0	$\cos^2(2\pi x_{Ce})M_y^2$	M_x^2
Γ_6	0	$\sin^2(2\pi x_{Ce})M_z^2$	0
Γ_7	$\cos^2(2\pi y_{Ce})M_z^2$	$\cos^2(2\pi x_{Ce})M_z^2$	0
Γ_8	$\sin^2(2\pi y_{Ce})M_x^2$	$\sin^2(2\pi x_{Ce})M_y^2$	0

M_x, M_y and M_z are the magnetic moment's components (Table 3).

observed] and the magnetic structures listed in Table 3, magnetic structure factors $\langle \mathbf{F}_M(\mathbf{K}) \cdot \mathbf{F}_M(\mathbf{K})^* \rangle$ have been calculated:

$$\mathbf{F}_M(\mathbf{K}) = \frac{1}{8}\sum_{i=1}^{8}\left(\mathbf{M}_i - \frac{(\mathbf{M}_i \cdot \mathbf{K})\mathbf{K}}{\mathbf{K}^2}\right)\exp(2i\pi\mathbf{K}\cdot\mathbf{r}_i), \quad (1)$$

(Γ_1–Γ_8) for $(0\,1\,0)_M$, $(1\,0\,0)_M$ and $(0\,0\,1)_M$ Bragg reflections. $\mathbf{F}_M(\mathbf{K})$, the magnetic structure factor at $\mathbf{K} = h\mathbf{a}^* + k\mathbf{b}^* + l\mathbf{c}^*$, is defined as: the summation being over 8 Ce atoms in Ibam unit cell; $\mathbf{r}_i$ are the corresponding atomic positions and $\mathbf{M}_i$, the associated magnetic moments. As atoms related via $[\frac{1}{2}\frac{1}{2}\frac{1}{2}]$ are opposite, $\mathbf{F}_M(\mathbf{K})$ can be written as

$$\mathbf{F}_M(\mathbf{K}) = \frac{1}{8}[1-(-1)^{h+k+l}] \times \sum_{i=1}^{4}\left(\mathbf{M}_i - \frac{(\mathbf{M}_i \cdot \mathbf{K})\mathbf{K}}{\mathbf{K}^2}\right)\exp(2i\pi\mathbf{K}\cdot\mathbf{r}_i). \quad (2)$$

Table 4 lists the results of $\langle \mathbf{F}_M(\mathbf{K}) \cdot \mathbf{F}_M(\mathbf{K})^* \rangle$ [$\langle\ \rangle$ being the mean value over $(h\,k\,l)$ multiplicity], for Γ_1–Γ_8 irreducible representation and $(0\,1\,0)_M$, $(1\,0\,0)_M$ and $(0\,0\,1)_M$ magnetic Bragg peaks. As $(0\,1\,0)_M$ exists, but neither $(1\,0\,0)_M$ nor $(0\,0\,1)_M$ is present at low temperature, Γ_1, Γ_2, Γ_5, Γ_6 (Fig. 5a), Γ_{3b} and Γ_{8b} (Fig. 5b) are to be excluded as candidates for $Ce_2Ni_3Ge_5$ magnetic structure. At this first level for selection, Γ_4, Γ_7, Γ_{3a} and Γ_{8a} (Fig. 5b) are still candidates, and they have to be "distinguished" via $(1\,1\,1)_M$ and $(2\,1\,0)_M$ magnetic contributions: Γ_{3a} and Γ_{8a} (Fig. 5b) are the only structures giving rise only to $(0\,1\,0)_M$ and $(1\,1\,1)_M$ magnetic Bragg peaks.

As waited for, the best fit between experimental and calculated neutron diffraction patterns (difference of the patterns recorded, respectively, at 1.4 and 6 K) is obtained either for Γ_3 or Γ_8 magnetic arrangement, with Ce magnetic moments parallel to the **a**-axis: the ordered magnetic moment is refined to be $0.4(1)\,\mu_B$ ($M_x = 0.4(1)\,\mu_B$ and $M_y = 0.0(1)\,\mu_B$), which is lower than the expected Ce^{3+} free ion value ($g_J J = 2.14\,\mu_B$). Let us note that the relatively high value for reliability factors R_M (R_M, respectively, equal to 28.2% and 22.4%) is a consequence of the very weak intensities of the magnetic reflections (Fig. 4).

The two possible $Ce_2Ni_3Ge_5$ collinear magnetic structures are represented in Fig. 6. These structures consist of a stacking of ferromagnetic $(0\,1\,0)$ planes with the $+\ +\ -\ -$ sequence along the **b**-axis. Note that they are closely related (they are identical if $x = \frac{1}{2}$ and $y = \frac{1}{2}$, one is deduced from the other by a shift along **b**-axis by one $(0\,1\,0)$ plane. A similar result was reported for the equivalent ternary germanide $U_2Rh_3Si_5$ but in this case the two possible magnetic structures are non-collinear [19].

The small ordered magnetic moment $(0.4(1)\,\mu_B)$ observed in $Ce_2Ni_3Ge_5$ indicates that the influence of Kondo effect is strong in this ternary germanide. This result is consistent with the explanation reported by Hossain et al. [8] classifying this compound as a Kondo lattice (large negative paramagnetic Curie temperature $\theta_p = -52$ K, increase of electrical resistivity below 30 K followed by a strong decrease around 5.1 K). All these properties suggest a large Kondo temperature T_K implying a strong reduction of the ordered magnetic moment of Ce atoms in $Ce_2Ni_3Ge_5$. Certainly in this ternary germanide, the magnetic ordering appears in the quantum regime where $T_N \ll T_K$. In other words, the replacement of Ni by Ge according to the sequence $CeNi_2Ge_2 \rightarrow Ce_2Ni_3Ge_5$ (or $CeNi_{1.5}Ge_{2.5}$) induces a non-magnetic $\rightarrow$ antiferromagnetic transition but the Kondo effect is still present. Let us note that an increase of ordered magnetic moment of Ce atoms was also observed for a comparable sequence: $CePd_2Ge_2$ $(0.85(5)\,\mu_B) \rightarrow Ce_2Pd_3Ge_5$ $(1.25(5)\,\mu_B)$

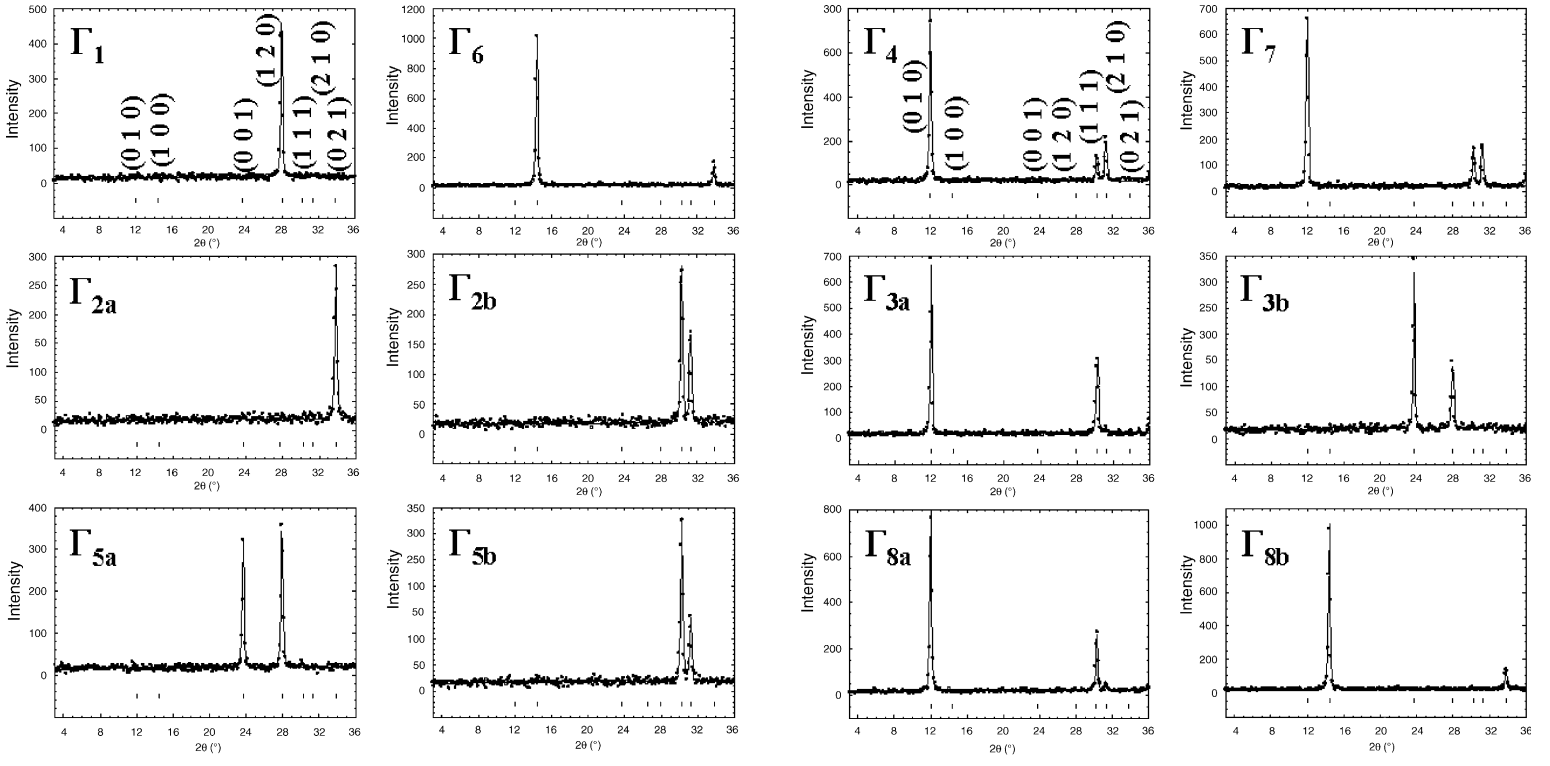

Fig. 5. Neutron powder diffraction patterns calculated (these diagrams are all calculated for the same value of the Ce magnetic moment) for: (a) Γ_1 and Γ_6 (magnetic moments parallel to **c**-axis), Γ_2 and Γ_5 (magnetic moment perpendicular to **c**-axis) magnetic structures; for the sake of clarity, the components of the magnetic moments, respectively, parallel to **a**- and **b**-axis have been considered independently and the resulting diagrams are labelled Γ_{2a}, Γ_{5a}, Γ_{2b} and Γ_{5b}; (b) Γ_4 and Γ_7 (magnetic moments parallel to **c**-axis), Γ_3 and Γ_8 (magnetic moment perpendicular to **c**-axis) magnetic structures; for the sake of clarity, the components of the magnetic moments, respectively, parallel to **a**- and **b**-axis have been considered independently and the resulting diagrams are labelled Γ_{3a}, Γ_{8a}, Γ_{3b} and Γ_{8b}.

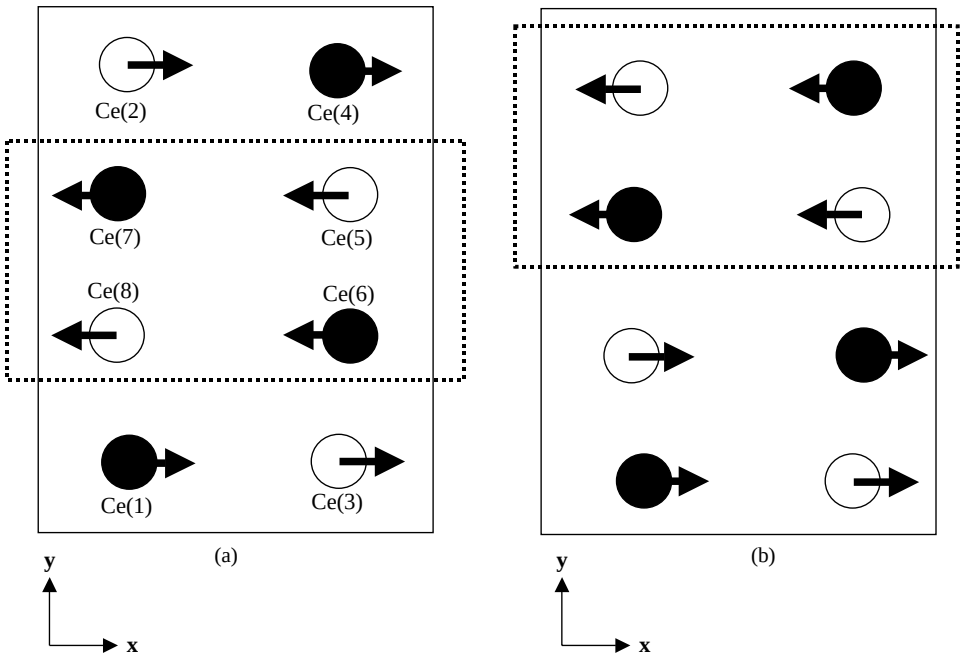

Fig. 6. Magnetic structures of $Ce_2Ni_3Ge_5$ projected onto the (0 0 1) plane corresponding to: (a) Γ_3 and (b) Γ_8 irreducible representations. Ce atoms are represented by black circles when $z = 0$ or 1 and white circles when $z = \frac{1}{2}$. The dotted zones represent the ferromagnetic layers and the solid line represents the unit cell unit.

and ascribed to a reduction of the influence of the Kondo effect [20].

4. Conclusion

Magnetisation measurements suggest the occurrence of two magnetic transitions at $T_{N1} = 4.8(2)$ K and $T_{N2} = 4.2(2)$ K for $Ce_2Ni_3Ge_5$. This behaviour seems to be confirmed by specific heat measurements [8]. But neutron powder diffraction (this work) detects only one magnetic transition (T_{N1}). The origin of the second transition (T_{N2}) is not explained at present. We have found that Ce atoms in $Ce_2Ni_3Ge_5$ carry an ordered magnetic moment of only $0.4(1)\,\mu_B$ revealing the strong influence of Kondo effect on the physical properties of this ternary germanide. A single crystal neutron diffraction would be necessary to test the existence of a change in $Ce_2Ni_3Ge_5$ magnetic structure at T_{N2}.

References

[1] B. Chabot, E. Parthé, J. Less-Common Met. 97 (1984) 285.
[2] P. Salamakha, M. Konyk, O. Sologub, O. Bodak, J. Alloys Compounds 236 (1996) 206.
[3] C. Godart, L.C. Gupta, C.V. Tomy, S. Patil, R. Nagarajan, E. Beaurepaire, R. Vijayaraghavan, J.V. Yakhmi, Mater. Res. Bull. 23 (1988) 1781.
[4] B. Becker, S. Ramakrishnan, D. Groten, S. Süllow, C.C. Mattheus, G.J. Nieuwenhuys, J.A. Mydosh, Physica B 230–232 (1997) 253.
[5] C. Mazumdar, R. Nagarajan, C. Godart, L.C. Gupta, B.D. Padalia, R. Vijayaraghavan, J. Appl. Phys. 79 (1996) 6347.
[6] Z. Hossain, H. Ohmoto, K. Umeo, F. Iga, T. Suzuki, T. Takabatake, N. Takamoto, K. Kindo, Phys. Rev. B 60 (1999) 10383.
[7] B. Chevalier, J. Etourneau, J. Magn. Magn. Mater. 196–197 (1999) 880.
[8] Z. Hossain, S. Hamashima, K. Umeo, T. Takabatake, C. Geibel, F. Steglich, Phys. Rev. B 62 (2000) 8950.
[9] S.J.S. Lister, F.M. Grosche, F.V. Carter, R.K.W. Haselwinner, S.S. Saxena, N.D. Mathur, S.R. Julian, G.G. Lonzarich, Z. Phys. B 103 (1997) 263.

[10] P. Gegenwart, F. Kromer, M. Lang, G. Sparn, C. Geibel, F. Steglich, Phys. Rev. Lett. 82 (1999) 1293.
[11] L. Durivault, F. Bourée, B. Chevalier, G. André, J. Etourneau, O. Isnard, J. Magn. Magn. Mater. 232 (2001) 139.
[12] H.M. Rietveld, J. Appl. Crystallogr. 21 (1969) 65.
[13] J. Rodriguez-Carvajal, Powder diffraction, Satellite Meeting of the 15th Congress of IUCr, Toulouse, France, 1990, p. 127.
[14] V.F. Sears, Neutron News 3 (1992) 26.
[15] A.J. Freeeman, J.P. Desclaux, J. Magn. Magn. Mater. 12 (1979) 11.
[16] B. Chabot, E. Parthé, J. Less-Common Met. 97 (1984) 285.
[17] E.I. Gladyshevsky, O.I. Bodak, V.K. Pecharsky, in: K.A. Gschneidner Jr, L. Eyring (Eds.), Handbook on the Physics and Chemistry of Rare Earths, Vol. 13, Elsevier, Amsterdam, 1990, pp. 01–190.
[18] E.F. Bertaut, Acta Crystallogr. A 24 (1968) 217.
[19] R. Feyerherm, B. Becker, M.F. Collins, J. Mydosh, G.J. Nieuwenhuys, S. Ramakrishnan, Physica B 234–236 (1997) 891.
[20] R. Feyerherm, B. Becker, M.F. Collins, J. Mydosh, G.J. Nieuwenhuys, S. Ramakrishnan, Physica B 241–243 (1998) 643.